

# Development of an acrylamide-based inhibitor of protein S-acylation

Saara-Anne Azizi<sup>1,2,#</sup>, Tong Lan<sup>1,#</sup>, Clémence Delalande<sup>1</sup>, Rahul S. Kathayat<sup>1</sup>, Fernando Banales Mejia<sup>1</sup>, Alice Qin<sup>1</sup>, Noah Brookes<sup>1</sup>, Perla Jasmine Sandoval<sup>1</sup>, Bryan C. Dickinson<sup>1,\*</sup>

<sup>1</sup>Department of Chemistry, The University of Chicago, Chicago, Illinois 60637, United States

<sup>2</sup>Medical Scientist Training Program, Pritzker School of Medicine, The University of Chicago, Chicago, Illinois 60637, United States

\*Dickinson@uchicago.edu

#These authors contributed equally to this work.

## Abstract

Protein S-acylation is a dynamic lipid post-translational modification that can modulate the localization and activity of target proteins. In humans, the installation of the lipid onto target proteins is catalyzed by a family of 23 Asp-His-His-Cys domain-containing protein acyltransferases (DHHC-PATs). DHHCs are increasingly recognized as critical players in cellular signaling events and in human disease. However, progress elucidating the functions and mechanisms of DHHC “writers” has been hampered by a lack of chemical tools to perturb their activity in live cells. Herein, we report the synthesis and characterization of **cyano-myracrylamide (CMA)**, a broad-spectrum DHHC family inhibitor with similar potency to 2-bromopalmitate (2BP), the most commonly used DHHC inhibitor in the field. Possessing an acrylamide warhead instead of 2BP’s  $\alpha$ -halo fatty acid, **CMA** inhibits DHHC family proteins *in cellulo* while demonstrating decreased toxicity and avoiding inhibition of the S-acylation eraser enzymes – two of the major weaknesses of 2BP. Our studies show that **CMA** engages with DHHC family proteins in cells, inhibits protein S-acylation, and disrupts DHHC-regulated cellular events. **CMA** represents an improved chemical scaffold for untangling the complexities of DHHC-mediated cell signaling by protein S-acylation.

## Introduction

Protein S-acylation is the post-translational addition of a long chain fatty acid to cysteine thiols via a thioester bond<sup>1-2</sup> and is often referred to as S-palmitoylation due to the prevalence of C16:0 modification. S-acylation has complex and wide-ranging effects on target proteins; not only can it alter membrane association and subcellular trafficking, as for the well-studied oncogene Ras<sup>3</sup>, but it also regulates protein oligomerization, activity, and stability<sup>3-7</sup>. S-acylation is enzymatically reversible, with lipid addition catalyzed by the protein acyl transferases (PATs), which possess an active site Asp-His-His-Cys domain (earning them the moniker “DHHC”) and lipid removal, by a suite of serine hydrolase family acyl-protein thioesterases (APTs), including APT1<sup>8</sup>, APT2<sup>9</sup>, ABHD10<sup>6</sup>, and ABHD17A/B/C<sup>10</sup>. The activity of both these DHHC “writer” and APT “eraser” proteins is tightly regulated, and together, they in turn dynamically regulate protein S-acylation. Disruption of this cycle is consequential at the cellular and organismal levels<sup>11-13</sup>.

In particular, dysregulation of DHHC family proteins is associated with human pathology, including cancer progression, inflammation, and neurological dysfunction<sup>14-16</sup>. For example, zDHHC9 is upregulated in colorectal cancer and has been implicated in the pathogenesis of leukemia<sup>17-18</sup>, while its loss-of-function mutations are associated with X-linked intellectual disability (XLID)<sup>19-20</sup>. ZDHHC20 regulates the signaling of the receptor tyrosine kinase EGFR, and its activity has been implicated in cellular transformation and lung tumorigenesis<sup>21-22</sup>. Finally, knockdown of zDHHC7 has been shown to mitigate symptoms of inflammatory bowel disease, possibly via loss of STAT3 palmitoylation and activation<sup>23</sup>.

Despite the annotation of the first palmitoyl transferase in yeast two decades ago<sup>24-25</sup>, a paucity of tools to perturb the function of the DHHC family has hindered progress in our understanding of their mechanism, regulatory roles, and connections to disease states. Functional redundancy between many DHHCs, as well as inter-family regulation<sup>26-28</sup>, limit the use of classic genetic tools and highlight the necessity of small molecule inhibitors. While the  $\alpha$ -brominated fatty acid 2-bromopalmitate (2BP) is the most commonly used small molecule tool to study DHHC functions in live cells, its frequent use obscures its promiscuity, poor utility, and cellular toxicity. 2BP is hypothesized to act as a pan-DHHC inhibitor by covalently modifying the active cysteine residues of DHHC proteins, either as 2BP or the 2BP-CoA adduct, with the latter metabolic product displaying enhanced reactivity with proteome<sup>29</sup>. In fact, 2BP inhibits at least two of the S-acylation erasers, APT1 and APT2, in cells<sup>30</sup>. Moreover, 2BP is often used at micromolar concentrations (10-100  $\mu$ M), concentrations that are at or above its toxicity threshold<sup>27, 29, 31</sup>. Other reported S-

acylation inhibitors, such as cerulenin, tunicamycin, and compound V, suffer from significant toxicity, poor selectivity, and/or a lack of characterization in cells<sup>32-34</sup>. Thus, there is a critical need for new chemical probes to study DHHC-mediated S-acylation in endogenous contexts.

Here, we report the development of **CMA**, a covalent broad-spectrum DHHC inhibitor with an acrylamide warhead and improved properties relative to 2BP. Not only is **CMA** more potent than 2BP *in vitro*, it is also less toxic and does not inhibit APT1 or APT2, thereby addressing two key limitations of 2BP. We demonstrate that **CMA** inhibits S-acylation and engages directly with DHHC family proteins *in cellulo*. Finally, we show that **CMA** can modulate DHHC-dependent cellular effects, including EGFR-mediated cell signaling and CD36-mediated lipid uptake and droplet formation. Overall, this work introduces **CMA** as a chemical tool that inhibits a broad range of DHHCs and complements current methods to study the biological implications of disrupting DHHC-mediated S-acylation.

### Acrylamide-based molecules inhibit zDHHC20

The DHHC family proteins are thought to employ a two-step mechanism, in which the cysteine thiolate of the active site attacks the fatty acyl-CoA thioester, resulting in an autoacylated DHHC with the acyl chain bound in the hydrophobic groove. The fatty acyl chain is then transferred from the cysteine to a protein substrate. This nucleophilic cysteine can be targeted by electrophiles – like 2BP – to hamper DHHC activity. In pursuit of a still potent but less reactive inhibitor *in cellulo*, we proposed to exchange the  $\alpha$ -halo carbonyl of 2BP with an acrylamide warhead. Acrylamides are known to react faster with cysteine thiols than serine alcohols, and, unlike the 2BP fatty acid, will likely not undergo metabolic conversion to reactive and nonspecific acyl CoA intermediates<sup>29, 35</sup>. Moreover, the acrylamide scaffold is achiral and readily synthetically accessible. Therefore, we designed and synthesized **1** (**Figure 1A**), which features a 14 carbon-long lipid tail appended to the acrylamide warhead. Docking of **1** on the only published crystal structure of a human DHHC (zDHHC20) showed that the warhead is proximal (3.5 Å) to the active site Cys (**Figure S1**). We therefore tested **1** against purified zDHHC20 using a fluorescence polarization (FP) assay adapted from Acyl-cLIP and using a fluorophore-tagged peptide that we identified as a substrate of zDHHC20, 5-FAM-NRas (**Figure S2**)<sup>36</sup>. **1** ( $IC_{50} = 21.4 \pm 5.9 \mu\text{M}$ ) successfully inhibited zDHHC20, although with decreased activity as compared to 2BP ( $IC_{50} = 5.33 \pm 0.77 \mu\text{M}$ ), confirming that an acrylamide-based lipid inhibitor can inhibit zDHHC20. Thus, we decided to explore the structure-activity relationship of **1** in an effort to enhance its potency.

### **CMA is a potent zDHHC20 inhibitor**

To optimize **1**, we designed and synthesized a panel of compounds, all with an acrylamide appended to a lipid tail. First, we targeted the lipid tail, shortening it by four carbons (**2**). This change abrogated the zDHHC20 inhibitory properties entirely, demonstrating the criticality of extensive contacts with the hydrophobic channel and inspiring us to instead focus on modifying the acrylamide moiety. We next tested compounds with either a substituted acrylamide amine and/or a butenoic acid-modified amide (**Figure 1B**). While most performed worse than the parent molecule, one molecule functionalized with a cyanomethyl group, **CMA**, showed significantly improved activity against zDHHC20, with approximately 80% inhibition at 10  $\mu\text{M}$ . **CMA** was found to have an  $\text{IC}_{50}$  of  $1.35 \pm 0.26 \mu\text{M}$  against zDHHC20 with 1 hour of preincubation, a 5-fold improvement over 2BP (**Figure S3**). We further characterized the kinetic parameters of covalent modification,  $k_{\text{inact}}$  and  $K_{\text{I}}$  for both **CMA** and 2BP, observing that **CMA** had both a faster reaction rate (2.08 vs. 1.35  $\text{min}^{-1}$ ) and a stronger affinity towards zDHHC20 (5.8 vs. 6.4  $\mu\text{M}$ ) than 2BP (**Figure S4**). Moreover, addition of the cyanomethyl group to the *cis* butenoic acid derivative (**3**) improved its activity (**12**), highlighting the criticality of this moiety. A second molecule, **8**, which possesses a terminal alkyne in lieu of the cyanomethyl, was similar in potency to 2BP, with an  $\text{IC}_{50}$  of  $8.32 \pm 2.25 \mu\text{M}$  (**Figure S3**). To confirm that the reactivity of **CMA** and **8** stemmed from the acrylamide warhead and not reversible thioimidate complex formation, we synthesized and tested **13** and **14**, the alkyl amide analogues of **8** and **CMA**, respectively (**Figure 1B**). Both molecules were inactive, verifying the acrylamide as the DHHC-reactive moiety. In sum, **CMA** is a potent zDHHC20 inhibitor *in vitro* and requires both the cyanomethyl group and acrylamide warhead for activity. Therefore, to assess its utility in live cells, we next assessed its inhibition of APTs and toxicity.

### **CMA does not inhibit APTs and is less toxic than 2BP**

To determine if **CMA** inhibits eraser APTs, as observed with 2BP, we evaluated the effects of **CMA** relative to 2BP on APT1 and APT2 activity *in vitro* using a fluorogenic probe for APT activity, DPP5<sup>37</sup>. **CMA** showed little inhibition of APT1 and APT2, while 2BP, in agreement with previous reports, significantly inhibited both APT1 and APT2 (**Figure 2A**)<sup>30</sup>. At 25  $\mu\text{M}$ , a concentration at or below which 2BP is often used, 2BP abolished most activity of APT1 and all activity of APT2. In striking contrast, **CMA** showed no inhibition of APT1 or APT2 even at 50  $\mu\text{M}$ , the highest concentration assayed. This data suggests that **CMA**, unlike 2BP, can be used to monitor the dynamics and the kinetics of acylation without perturbing APT-mediated deacylation.

We also compared the toxicity of **CMA** to that of 2BP across a panel of commonly used mammalian cell lines, including MDA-MB-231, HEK293T, and 3T3-L1. After 24 hours of treatment, **CMA**'s toxicity was limited up to 40  $\mu$ M, while 2BP significantly reduced cell viability at much lower concentrations (**Figure 2B, S5**). For example, in MDA-MB-231 cells, treatment with 2BP resulted in ~90% cell death at 20  $\mu$ M, whereas at the same concentration of **CMA**, no toxicity was observed. However, as the toxicity of both compounds was cell-line dependent, **CMA** treatment time and concentration will need to be optimized for a particular experimental system. As **CMA** was non-toxic at 20  $\mu$ M across all cell lines we tested, we designated this as our maximum concentration of **CMA** to use for assessment in these cell lines. Overall, these results – the lack of APT inhibition and decreased toxicity – paired with the robust inhibition of zDHHC20 *in vitro*, suggested that **CMA** might be an inhibitor of zDHHC-mediated acylation in cells.

### **CMA inhibits protein S-acylation in live cells**

To validate the use of **CMA** as an inhibitor of S-acylation, we next sought to assess its efficacy and potency in live cells. Using 17-octadecynoic acid (17-ODYA) metabolic labeling, wherein a clickable fatty acid is used to monitor lipid incorporation, we observed a dose-dependent decrease in global S-acylation when cells were treated with **CMA** (**Figure 3A, S6**)<sup>38</sup>. We further confirmed the global inhibition of protein S-acylation by **CMA** using acyl-biotin exchange (ABE)<sup>39</sup>, a method for the enrichment and visualization of acylated cysteine residues (**Figure 3B, S7**).

To corroborate these proteome-wide observations and also to evaluate the conditions of **CMA** inhibition, we next tested whether and when **CMA** could inhibit the S-acylation of several well-studied DHHC substrate proteins. We first assessed its effect on the S-acylation status of overexpressed Legionella E3 ligase GobX, the overexpressed human immune adaptor protein Myd88, and the endogenous GTPase Ras, which are regulated by zDHHC20, zDHHC9, and zDHHC6, respectively<sup>40-41</sup>. After treating HEK293T cells with a range of concentrations of **CMA** under serum-free conditions, we observed a dose-dependent decrease in the S-acylation of overexpressed GobX and Myd88 and endogenous Ras, with a significant loss of acylation at 20  $\mu$ M after 6 hours of treatment for all three substrates (**Figure 3C**). We then assessed the time course of **CMA** inhibition of these two targets at 0, 1, 3, and 6 hours, observing significant inhibition for these particular substrates only after 6 hours of treatment (**Figure S8**). However, as the turnover of acylation is substrate-dependent, the time component of **CMA** inhibition will need to be optimized for individual substrates<sup>42-43</sup>. Additionally, as the non-specific binding with serum proteins in culture media is a known challenge for small molecule inhibitors, we also assayed the

effect of serum concentration on **CMA** alongside 2BP, probing both global and GobX S-acylation. Using ABE, we observe that in up to 1% FBS, both **CMA** and 2BP inhibit global and GobX S-acylation, but with 10% FBS, the activity of both molecules appears extremely limited (**Figure 3D, S9**). Overall, all targets displayed reduced acylation at a concentration of 20  $\mu$ M **CMA** with 6 hours of treatment, establishing this as our working concentration. Collectively, these data confirm that **CMA** inhibits protein S-acylation in live cells.

### **CMA engages DHHCs in live cells**

Having verified that **CMA** inhibits zDHHC20 *in vitro* and blocks protein S-acylation in live cells, we next sought to confirm direct engagement of DHHC family proteins by **CMA** in live cells. We postulated that **8**, an analogue of **CMA** possessing a terminal alkyne instead of the cyanomethyl group, could be used to visualize **CMA** engagement across the DHHC family by reporter conjugation via copper-catalyzed azide-alkyne “click” cycloaddition (**Figure 1A**). Therefore, we first visualized **8** labeling across the proteome, subjecting **8**-treated HEK293T cell lysates (10  $\mu$ M, 2 hours) to the click reaction with TAMRA-azide. In-gel fluorescence indicated labeling in both serum-free and 10% FBS-complemented media, although labeling rate and intensity were decreased under the latter conditions (**Figure S10**). We next determined which DHHCs could be labeled by **8**. HEK293T cells overexpressing individual DHHCs were treated with **8** (10  $\mu$ M, 2 hours), and, as above, following cell lysis, subjected to a click reaction with TAMRA-azide in order to label **8**-modified proteins. Analysis of in-gel fluorescence showed that **8** labels zDHHC2, 4, 6, 9, 11, 13, 14, 15, 16, 18, 20, 23, and 24, all of the DHHCs in our human and murine libraries with strong expression (**Figure S10A-C, 11**). Furthermore, **8** was also found to label endogenous DHHC proteins, including zDHHC5 and 7, which was not labeled in the fluorescence screen, likely due to poor expression (**Figure S12**). Notably, the labeling intensity and range of **8** differed from 16C-BYA, possibly suggesting different selectivity profiles for **CMA** and 2BP.

We next examined the residues of DHHC proteins labelled by **8**. As the cysteine residue within the DHHC motif is critical for the S-acyltransferase activity for DHHC proteins<sup>24-25, 44-45</sup>, we performed **8** labeling on a subset of exogenous catalytically dead (DHHS) mutants. While some DHHCs, such as zDHHC9 and 24, evinced decreased labeling of the active site mutant, other DHHCs, including zDHHC20, did not, suggesting that the DHHC motif Cys is not the only residue modified by **8**, as is also observed with 16C-BYA, an alkyne-containing analogue of 2BP<sup>46</sup> (**Figure S13**). While the functional consequences of the 2BP and **CMA** reactivity with peripheral cysteines

remain unknown, this result could suggest a possible role for these residues in the mechanism of inhibition.

The background fluorescence observed during in-gel labeling with **8** suggested that **CMA** has off-targets in cells. Thus, we decided to use mass spectrometry (MS) to profile the proteome-wide reactivity of **8** and therefore **CMA**. To this end, following treatment of HEK293T cells with 20  $\mu$ M **8** or DMSO, click reaction with biotin-azide, enrichment, and on-bead trypsin digestion, digested peptides were identified and quantified by dimethyl labeling. Consistent with the gel-based results, we found that **8** had a wide range of off-targets in cells (**Figure S15, Table S1**). When filtered with  $\geq 2$  unique peptides and  $\geq 5$ -fold enrichment in at least 2 of 3 replicates, 271 targets can be identified. Top enriched proteins include chitobiosyldiphosphodolichol beta-mannosyltransferase (ALG1), threonylcarbamoyl adenosine tRNA methylthiotransferase (CDKAL1), and neutral cholesterol ester hydrolase 1 (NCEH1), while off-targets (targets other than DHHC family members) more broadly included transferases, translocases, and channel proteins. Unsurprisingly, due to the low abundance and have high hydrophobicity of DHHC family proteins, LC-MS/MS analysis only identified one DHHC protein (zDHHC6), which did not even pass the threshold when the enrichment cutoff was set to 5 (**Figure S15, Table S1**)<sup>29, 46-48</sup>. Overall, we hope that this proteomics data can provide a guide for optimizing future derivatives of **CMA** against off-targets.

Having profiled the reactivity of **8** and validated its ability to label DHHC family proteins, we next performed competitive labeling with **CMA** for exogenous (zDHHC2, zDHHC9, zDHHC14, zDHHC15, and zDHHC24) and endogenous (zDHHC5, 13, and 18) DHHC proteins labeled by **8** in order to confirm **CMA** target engagement in live cells. For the exogenous DHHCs, cells overexpressing each targeted protein were treated with **CMA** (0, 10, and 20  $\mu$ M, 2 hours) in either serum-free or 10% FBS media, chased with **8** (1  $\mu$ M, 2 hours), and then lysed. After TAMRA-azide ligation, in-gel fluorescence indicated that **CMA** blocked **8** labeling, confirming that **CMA** engages each of these DHHC targets (**Figure 4A, S10D, S14**). To probe the endogenous DHHCs, we again performed competitive labeling, this time on non-transfected HEK293T cells and using **8** at 20  $\mu$ M for 3 hours for the chase. Here, after conjugation with biotin-azide, pulldown, and Western blotting, we observed that **CMA** impeded the **8** labeling of zDHHC5, zDHHC18, and two isoforms of zDHHC13 (**Figure 4B**) – confirming **CMA** directly engages with these DHHCs as well. The ability of **CMA** to outcompete **8** labeling of both exogenous and endogenous DHHCs

suggests that **CMA** inhibition of S-acylation in live cells likely stems from inhibition of DHHC family proteins.

### **CMA inhibits the S-acylation of EGFR and CD36**

Finally, we sought to test whether **CMA** could recapitulate observations reported to stem from DHHC disruption and establish that, along with on-target binding, **CMA** can be used to discern cellular outcomes from loss of S-acylation. A critical S-acylated protein and substrate of zDHHC20 is the epidermal growth factor receptor (EGFR), a receptor tyrosine kinase whose activity is widely dysregulated in cancer<sup>21</sup>. There are several mechanisms by which its C-terminal acylation regulates its activity; in a KRAS-mutant context, loss of its palmitoylation is reported to disrupt signaling along the phosphatidylinositol 3-kinase (PI3K) pathway<sup>22</sup>. Thus, we first confirmed that **CMA** diminished EGFR S-acylation in MDA-MB-231 cancer cells at its working concentration, but that **14**, the non-covalent analogue of **CMA** did not (**Figure 5A, S16**). We then assessed whether **CMA**-mediated interruption of EGFR acylation impacted downstream PI3K pathway signaling. We observed that treatment with **CMA**, but not with **14**, moderated the phosphorylation of protein kinase B (Akt) and the abundance of the transcription factor MYC, two markers of EGFR-P13K pathway activity (**Figure 5B, S17**). Interestingly, treatment with **10**, a molecule inactive against zDHHC20 *in vitro*, inhibited EGFR acylation and PI3K pathway activation *in cellulo*, possibly implicating another zDHHC in the regulation of the EGFR pathway (**Figure S16, 17C**). Overall, these results paralleled those seen with genetic knockdown of zDHHC20 and established **CMA**'s ability to validate results downstream of acylation disruption<sup>22</sup>.

To further substantiate **CMA**'s ability to modulate DHHC-dependent cellular functions, we next evaluated whether **CMA** could inhibit the S-acylation and subsequently the activity of CD36. CD36 is an immuno-metabolic glycoprotein and a substrate of zDHHC4 and zDHHC5, two DHHCs we confirmed were targeted by **CMA** (**Figure 4B, S11**). The S-acylation of CD36 mediates its localization and in turn its fatty acid translocase activity<sup>49</sup>. We found that treatment of 3T3-L1 pre-adipocytes with **CMA** not only reduced CD36 acylation levels (**Figure 5C**), but also decreased the uptake of fatty acids and formation of lipid droplets, results previously observed with knockdown of zDHHC4/5 (**Figure 5D, S19**). Together, these results indicate that not only does **CMA** perturb the acylation of significant endogenous targets, it also modulates their known acylation-dependent activity and functionality.

## Conclusions

As our understanding of the role of protein S-acylation in regulating cell and organismal biology grows, the toxicity and limited potency of current inhibitors demand improved chemical tools. In this Article, we introduced **CMA**, a broad-spectrum inhibitor of DHHC family proteins, to complement current methods to probe S-acylation and its consequences in cells. Featuring an acrylamide warhead functionalized with a cyanomethyl group, **CMA**'s potency is on par with 2BP – the leading inhibitor in the field – and, more importantly, has a significantly improved toxicity profile across multiple mammalian cells lines. We also show that **CMA** does not inhibit eraser APTs, a critical limitation of 2BP. These improvements were achieved without a loss of in-cell efficacy; for example, **CMA** inhibited the acylation of CD36 at 20  $\mu\text{M}$  under our conditions, while 2BP was used at 100  $\mu\text{M}$ <sup>49</sup>. Furthermore, we used **8**, an alkyne-containing derivative of **CMA**, to show that **CMA** engages with DHHC family proteins across clades, validating **CMA** as a broad-spectrum DHHC inhibitor and confirming its role in perturbing DHHC-dependent acylation. Finally, we applied **CMA** to assess cellular responses previously reported to result from loss of S-acylation. We demonstrated that decreases in the acylation of EGFR and CD36 caused by **CMA** treatment were paired with changes in signaling activity and lipid uptake, respectively – changes aligned with results reported using both genetic manipulation and 2BP treatment<sup>21, 27</sup>. These results not only emphasize the importance of S-acylation in biological processes, but also highlight the potential of **CMA** in elucidating the regulatory roles of DHHC family proteins.

While this work reveals the promise of acrylamide based DHHC family inhibitors, it also underscores the need for additional improvements in selectivity and potency. MS analysis suggests that **8** can label 271 proteins with high confidence in cells, over 75% of which are annotated as acylated proteins (**Table S1**). These results suggest that **8**, and in turn **CMA**, interact with acylated targets and emphasize the disadvantage of their lipid “tails.” As mimetics of fatty acids and their derivatives, aliphatic chains are thought to lead to numerous off-targets in cells<sup>50</sup>. Therefore, modification or replacement of the lipid will be critical in the next generation of molecules. As comparison of **1** with **2** indicates, though, the loss of hydrophobic contacts would need to be compensated for by expansion of the scaffold and increased contacts with the protein elsewhere. Interestingly, we observed that the cyanomethyl group was crucial for **CMA** potency; however, the reasons for its criticality are unclear. We envision that a crystal structure of a **CMA**-bound DHHC would both aid in deciphering the mechanism of the cyanomethyl-mediated increase in potency and highlight opportunities for structure-based design. The ability of **10** to inhibit S-acylation *in cellulo*, but not zDHHC20 *in vitro*, was also intriguing and suggests that some

members of our acrylamide panel might serve as a starting point for a DHHC inhibitor with intra-family specificity. In addition, the capability of zDHHC20 to acylate NRas peptide, as well as recent reports of DHHC-targeted peptide inhibitors, hint at the potential of peptide scaffolds as DHHC inhibitors<sup>51-52</sup>. Our future work will focus on modifying small molecule and peptide scaffolds to achieve improvements in selectivity and potency.

### **Acknowledgements**

This research was supported by the University of Chicago, the National Institute of General Medical Sciences of the National Institutes of Health NIH (R35 GM119840, to B.C.D.), the National Institute of Diabetes and Digestive and Kidney Diseases of the National Institutes of Health (F30 DK125088, to S-A.A.), and the Swiss National Science Foundation (P2BEP2\_188250, to C.D.). We thank the Mass Spectrometry Core facility at University of Illinois at Chicago for providing technical advice on sample preparation for proteomics. We thank S. Bamji (University of British Columbia), M. Fukata (NIPS, Japan), M. Machner (NIH) and B. Beutler (University of Texas Southwestern Medical Center) for providing the various plasmids used in this work.

### **Notes**

R.S.K. and B.C.D. have a patent on the DPP technology used in this work.

### **Supporting Information**

Supporting figures, tables, spectra, procedures, and analysis

## Methods

### ***In vitro* fluorescence polarization assay of zDHHC20 for molecule screening and IC<sub>50</sub> determination with 1-hour preincubation**

We used a 48  $\mu$ l protocol for initial molecule screening and IC<sub>50</sub> determination with 1 hour of preincubation. Purified zDHHC20 (64 nM in 12  $\mu$ L) in reaction buffer (50 mM HEPES, 150 mM NaCl, 1 mM EDTA, 2 mM TCEP, 2 mM DDM, pH 7.0) or reaction buffer with protein storage buffer was added to a 384-well optical bottom plate (ThermoFisher). 12  $\mu$ L of the small molecule stock in reaction buffer were added, resulting in a 24  $\mu$ L mixture of enzyme and small molecule, and the mixtures were incubated in 37 °C for 1 hour. The MasterMix II (24  $\mu$ L), containing 8  $\mu$ M palmitoyl-CoA and 2.5  $\mu$ M peptide 01(5-FAM-GTQGCMGLPCVVM-COOH) in reaction buffer, was added to initiate the reaction, resulting in 4  $\mu$ M and 1.25  $\mu$ M as the final concentration of palmitoyl-CoA and peptide 01, respectively. Fluorescence measurements were recorded on Synergy Neo2 Hybrid Multi-Mode Reader (BioTek Instruments, Inc.) with Dual FP Green filter cube. Fluorescence polarization ( $\lambda_{ex}$  = 485/20 nm,  $\lambda_{em}$  = 528/20 nm, gain=35, read from the top with height 7.5 mm, and filter switching method) was measured at 1-min time intervals for 2 hours at 37 °C. Assay data were exported in Microsoft Excel 2016. For all of the molecule screening and IC<sub>50</sub> determination, we performed the assay in kinetics mode, and data points at t=118 min were utilized as readout of enzyme activities of different samples for comparison.

### ***In vitro* assay of APT inhibition**

Purified APT1 or APT2 (200 nM in 75  $\mu$ L) in DPBS or DPBS alone was added to the 96-well optical bottom plate (ThermoFisher), followed by 75  $\mu$ L of 50, 100, or 200  $\mu$ M of 2BP or **CMA** in DPBS. Controls were incubated with an equal volume of DMSO. The mixtures were incubated in 37 °C for 1 hour. At the end of pre-incubation, 150  $\mu$ L of 2  $\mu$ M DPP-5 solution in DPBS was added, resulting in a final concentration of: 50 nM APT1/2; 1  $\mu$ M DPP-5; 0, 12.5, 25, 50  $\mu$ M 2BP or **CMA**. Fluorescence measurements were recorded on Synergy Neo2 Hybrid Multi-Mode Reader (BioTek Instruments, Inc.). Fluorescence intensities (excitation wavelength  $\lambda_{ex}$  = 490/20 nm, emission wavelength  $\lambda_{em}$  = 545/20 nm, gain=80, read from bottom with height 4.5 mm and sweep method) were measured at 15-second time intervals for 1 hour at 37 °C. The initial velocity was calculated from linear regression of the first 11 data points which was done using GraphPad Prism 8.

### **Acyl-biotin exchange (ABE) assay**

A 10 cm plate of cells was washed twice with cold DPBS, lysed with 1-2 mL of RIPA lysis buffer supplemented with a protease inhibitor cocktail and 50 mM *N*-ethylmaleimide (NEM) (Acros), and subjected to end-over-end rotation at 4 °C for at least three hours. Following centrifugation at 13,000g for 20 min. at 4 °C, the supernatant was collected. Protein concentration was measured using the BCA assay (ThermoFisher), and equal amounts of total protein from each sample were then subjected to acetone precipitation. The resulting pellet was dissolved by sonication in resuspension buffer (4% SDS, 50 mM HEPES, 150 mM NaCl, 5 mM EDTA, pH 7.4; 100 µL per mg of protein) containing 50 mM NEM, and then Triton buffer (0.2% Triton X-100, 50 mM HEPES, 150 mM NaCl, 5 mM EDTA, pH 7.4; 250 µL per mg of protein) containing 50 mM NEM was added. This protein solution was rotated end-over-end for 2-3 hours at 25 °C, followed by two chloroform–methanol precipitations to remove excess NEM. The resulting protein pellet was dissolved in 80 µL of resuspension buffer via sonication. The protein sample was divided into two equal parts for ±hydroxylamine (HA) (Combi-Blocks) treatment. Each sample was treated with 160 µL of either -HA buffer (Triton buffer) or +HA buffer (Triton buffer containing 0.7 M HA, pH 7.2-7.4). Samples were incubated for 1 hour at room temperature with shaking, and then proteins were precipitated by chloroform–methanol precipitation to remove excess HA. Protein pellets were resuspended by sonication in 40 µL of resuspension buffer containing 10 µM EZ-Link HPDP-Biotin (ThermoFisher), diluted with 160 µL of Triton buffer containing 10 µM HPDP-Biotin, and incubated for 2 hours at room temperature with shaking. Excess biotin was removed with two sequential chloroform-methanol precipitations. Protein pellets were dissolved in 40 µL resuspension buffer by sonicating, and the solution volume was brought to 400 µL with Triton buffer. Protein (25-25 µg) was removed to serve as an expression control ('input'). The remaining solution was diluted with Triton buffer, and streptavidin–agarose beads (50 µL of slurry per 1 mg of protein) were added to each sample, which were then incubated at 4 °C overnight with end-over-end rotation. Unbound proteins were removed by washing with 1 mL wash buffer (0.1% SDS, 0.2% Triton X-100, 50 mM HEPES, 150 mM NaCl, 5 mM EDTA, pH 7.4). Bound proteins ('output') were eluted by boiling the beads for 10 min at 95 °C with 1x Laemmli sample buffer (Alfa Aesar) containing 9% β-mercaptoethanol or 30 mM DTT. The protein was resolved on 8-12% SDS–PAGE gels and subjected to Western blotting using the protocol described above.

### **CMA ABE assay**

At 40-70% confluency, 10-cm plates of HEK293T cells were transfected with 4 µg pcDNA.6.1-eGFP-GobX or 6 µg pCMV-HA-Myd88 plasmid. At 24 hours post transfection, cells were treated

with **CMA** (0, 5, 10, and 20  $\mu$ M) for 6 hours. For endogenous targets, 10 cm dishes of MDA-MB-231 or 3T3-L1 preadipocytes at 80% confluency were treated with **CMA** (0, 20  $\mu$ M) for 3 or 6 hours. Cells were then lysed and samples prepared in accordance with the procedure described in the ABE protocol.

### **17-ODYA metabolic labeling assay**

HEK293T cells (~200,000 cells per well) were plated in 12-well plate (Fisher) in growth medium. After 48 hours, cells were treated with various concentrations of **CMA** or 2BP in serum-free DMEM for 3 hours. After 1 or 3 hours of preincubation, the media was replaced with metabolic labeling media (serum-free DMEM with 50 mM 17-ODYA preincubated with 5% BSA) complemented with the same concentration of either **CMA** or 2BP, and the cells were then incubated for another 6 hours. Cells were lysed by SDS-free lysis buffer (50 mM HEPES, 150 mM NaCl, 1% Triton-100, 0.5% sodium deoxycholate, pH=7.4). If no hydroxylamine treatment, after centrifugation, the final cell lysate was collected and normalized to 1 mg/ml in 30  $\mu$ L. For Cu-AAC conjugation, Master mix (2.4  $\mu$ L) made from equal volumes of 5 mM TAMRA-azide (click chemistry tools), 5 mM TBTA (Cayman), 50 mM CuSO<sub>4</sub>, and 50 mM TCEP was added into 30  $\mu$ L cell lysate. The resulting solution was incubated for 1 hour at room temperature in darkness, then the reaction was quenched with 6x Laemmli sample buffer containing 9%  $\beta$ -mercaptoethanol before running the SDS-PAGE gels. For hydroxylamine treatment, after centrifugation, the final cell lysate was collected and normalized to 1 mg/ml in 100  $\mu$ L. For Cu-AAC conjugation, Master mix (8  $\mu$ L) made from equal volumes of 5 mM TAMRA-azide (click chemistry tools), 5 mM TBTA (Cayman), 50 mM CuSO<sub>4</sub>, and 50 mM TCEP was added into 100  $\mu$ L cell lysate. The resulting solution was incubated for 1 hour at room temperature in darkness. The click reaction was quenched by chloroform-methanol precipitation. Each protein pellet was resuspended in resuspension buffer (the same in ABE assay), then was divided into two equal parts for  $\pm$  hydroxylamine (HA) treatment. Each sample was treated with 160  $\mu$ L of either -HA buffer (Triton buffer) or +HA buffer (Triton buffer containing 0.7 M HA, pH 7.2-7.4). Samples were incubated for 1 hour at room temperature with shaking, and then proteins were precipitated by chloroform-methanol precipitation to remove excess HA. Protein pellets were resuspended by sonication in 50  $\mu$ L of resuspension buffer and 6x Laemmli sample buffer containing 9%  $\beta$ -mercaptoethanol was added before running the gels. Proteins were resolved with 12% SDS-PAGE and visualized with FluoroChem R (Proteinsimple) using the MultiFluo-Green channel. Coomassie Blue was used to stain total protein.

### **MTS assay**

Cells (~100,000 cells per well for HEK293T, ~50,000 cells per well for 3T3-L1, MDA-MB-231, and HeLa, and ~70,000 cells per well for HepG2) were plated in 96-well plates (Corning) in growth media. After 24 hours, cells were washed once with DPBS and treated with **CMA** or 2BP in a concentration gradient for either 6 or 24 hours in serum-free DMEM (EMEM for HepG2 only). Then cells were washed by DPBS and then treated with the MTS reagent (Abcam) in serum-free DMEM GlutaMAX (EMEM, HepG2 only) for 2-3 hours. Absorption at 490 nm was measured on Synergy Neo2 Hybrid Multi-Mode Reader (BioTek Instruments, Inc.). The data are taken from at least  $n=2$  independent experiments containing at least two replicates each time. Assay data were analyzed using Microsoft Excel 2016 and nonlinear curve fitting was performed using GraphPad Prism 8.

### ***In cellulo* labeling assay of DHHC library**

HEK293T cells (~82,500 cells per well) were plated in 24-well plate (Fisher). For human DHHC labeling, after 20-24 hours, cells were transfected with 0.6  $\mu\text{g}$  plasmids with PEI. For mouse DHHC labeling, cells were transfected with 0.6  $\mu\text{g}$  plasmids with Lipofectamine 3000 (ThermoFisher) according to manufacturer's protocol. For **8** labeling assay, at 24 hours post transfection, cells were incubated with serum-free DMEM complemented with **8** for 2 hours. For **CMA** competitive labeling assay, at 24 hours post transfection, the media was removed, and cells were incubated with serum-free DMEM with **CMA** for 2 hours, then **8** in DMEM was added into media, resulting in a final concentration of **8** at 1  $\mu\text{M}$ . Cells then were washed with DPBS twice and lysed with 50  $\mu\text{L}$  RIPA buffer (50 mM HEPES, 150 mM NaCl, 1% Triton-100, 0.5% sodium deoxycholate, 0.1% SDS, pH=7.4). After spun down, the final cell lysate was collected and normalized to 1 mg/mL in 30  $\mu\text{L}$  before Cu-AAC conjugation. Cu-AAC conjugation with TAMRA-azide was performed according to the protocol shown above. Proteins were resolved with 12% SDS-PAGE and visualized with FluoroChem R (Proteinsimple) using the MultiFluo-Green channel. Western blots of anti-myc or anti-HA were used as a control to indicate the molecular sizes of DHHC proteins and the amount of DHHC proteins. Cells were labelled in serum-free media without further notice. When cells were labelled in serum-complemented media (0.1% or 1% FBS-complemented DMEM), for **8** labeling assay, at 24 hours post transfection, cells were incubated with DMEM complemented with **8** and corresponding concentration of FBS for 2 hours. For **CMA** competitive labeling assay, at 24 hours post transfection, the media was removed, and cells were

incubated with DMEM complemented with **CMA** and corresponding concentration of FBS for 2 hours, then **8** in DMEM was added into media, resulting in a final concentration of **8** at 10  $\mu$ M.

### ***In cellulo* labeling of endogenous DHHC proteins**

At 80-90% confluency, 10 cm dishes of HEK293T cells were incubated with DMSO or 20  $\mu$ M **CMA** in serum-free DMEM GlutaMAX for 3 hours, followed DMSO or 20  $\mu$ M **8** for an additional 3 hours. After treatment, cells were washed twice with cold DPBS and lysed in 1 mL of SDS-free RIPA buffer for 1 hour at 4 °C. Following centrifugation at 13,000g for 20 min. at 4 °C, the supernatant was collected, and protein concentration was determined using a BCA assay. Samples were normalized to 1 mg/mL. For Cu-AAC conjugation, a master mix (equal volumes of 5 mM biotin-azide (Click Chemistry Tools), 5 mM TBTA (Cayman), 50 mM CuSO<sub>4</sub>, and 5 mM TCEP) was prepared and added to each sample (16  $\mu$ L for 184  $\mu$ g protein). The resulting solution was rotated for 1 hour at room temperature and then quenched with 100 mM EDTA (100x) and subjected to two chloroform-methanol precipitations. Protein pellets were dissolved in 40  $\mu$ L ABE resuspension buffer by sonicating, and the total volume was brought to 400  $\mu$ L with ABE Triton buffer. Protein pellets were dissolved in 40  $\mu$ L resuspension buffer by sonicating, and the solution volume was brought to 400  $\mu$ L with Triton buffer. Protein (20-25  $\mu$ g) was removed to serve as an expression control ('input'). The remaining solution was diluted with Triton buffer, and streptavidin–agarose beads (50  $\mu$ L of slurry per 1 mg of protein) were added to each sample, which were then incubated at 4 °C overnight with end-over-end rotation. Unbound proteins were removed by washing three times with 1 ml of ABE wash buffer. Bound proteins ('output') were eluted by boiling the beads for 10 min at 95 °C with 1x Laemelli sample buffer (Alfa Aesar) containing 20-30 mM DTT. The protein was resolved on 8-12% SDS–PAGE gels and subjected to Western blotting using the protocol described above. For non-competitive **8** labeling, the **CMA** pretreatment step was not followed.

### **Lipid uptake assays**

On day 0, 3T3-L1 preadipocytes were plated at  $6.0 \times 10^4$  in an 8-well dish. On day 1, cells were cultured in serum-free media for 12 hours, and then, on day 2, treated with either **CMA** (20  $\mu$ M) or DMSO for 3 hours, followed by treatment with 10  $\mu$ M BSA-bound oleate and 2  $\mu$ M BODIPY 493/503 or BODIPY-palmitate for 6 hours. DAPI was then added, and then cells were washed and fixed with 4% paraformaldehyde. Cells were washed (5x5 min.) with PBS and mounted in Prolong Antifade Mountant (Thermo Fisher). Slides were imaged using an inverted epifluorescence microscope (Leica DMI8) equipped with a Hamamatsu Orca-Flash 4.0 camera, a 63x oil objective

(numerical aperture 1.4), and a 300 W Xenon light source (Sutter Lamba XL). LASX software was used to obtain BODIPY and brightfield images.



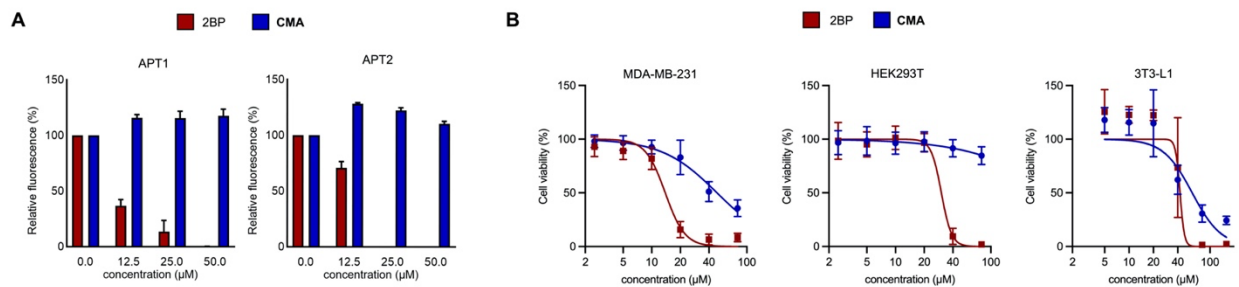


**Figure 2.** Characterization of **CMA** (A) Incubation of purified APT1 or APT2 (50 nM) with either 2BP or **CMA**, followed by measurement of APT activity using the fluorogenic probe DPP-5. Data are presented as the mean  $\pm$  standard deviation ( $n=3$ ). (B) Viability of HEK293T, MDA-MB-231, and 3T3-L1 cells treated with varied concentrations of either 2BP or **CMA** (24 hours), as measured by MTS assay. Data are presented as the mean  $\pm$  standard deviation ( $n \geq 3$ ).

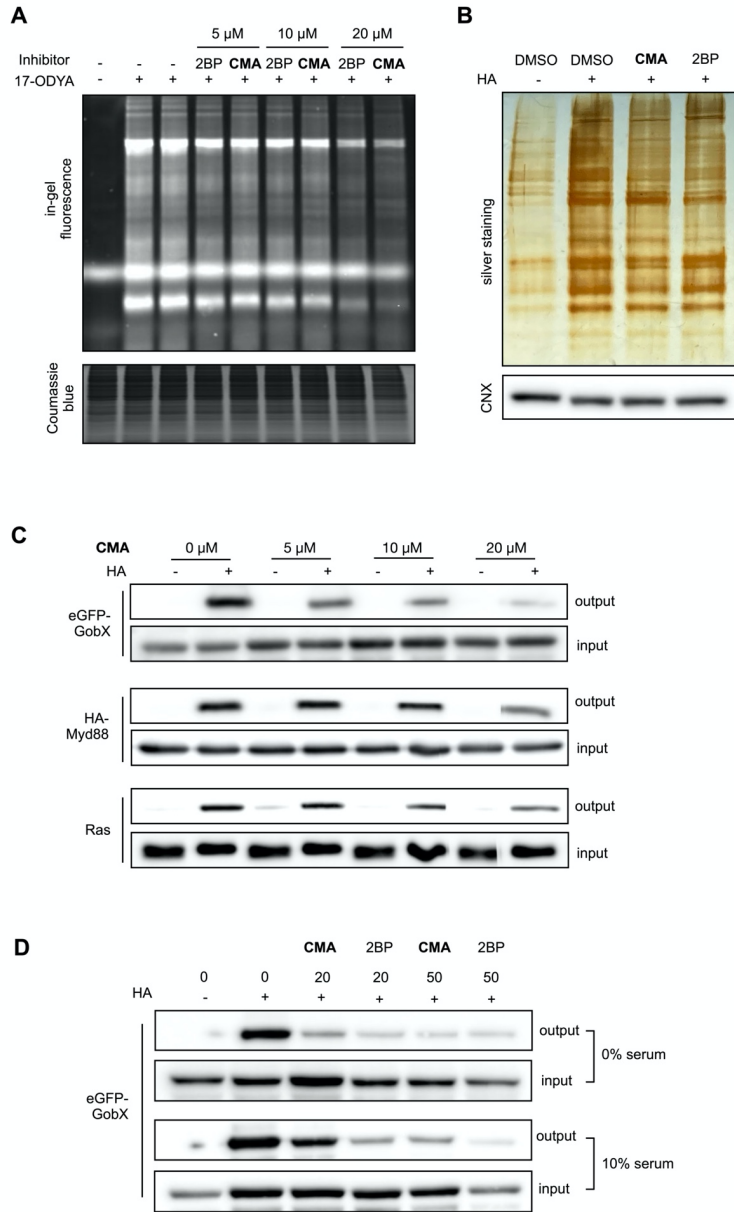


**Figure 3.** Validation of **CMA** *in cellulo* (A) HEK293T cells pretreated with DMSO, 2BP or **CMA** (0, 5, 10, and 20  $\mu$ M, 3 hours) before treatment with 17-octadecynoic acid (17-ODYA) (6 hours) to metabolically label palmitoylated proteins. Isolated proteomes were then subject to click chemistry to conjugate TAMRA-azide to proteins modified by 17-ODYA, followed by protein separation via SDS-PAGE. In-gel fluorescence revealed a proteome-wide decrease in protein palmitoylation with **CMA** treatment. (B) Acyl-biotin exchange (ABE) of HEK293T cells treated with 2BP or **CMA** (20  $\mu$ M, 6 hours). Global S-acylation visualized using silver staining, with CNX as a loading control ( $n \geq 2$ ). (C) Dose-response change in the S-acylation of exogenous eGFP-tagged GobX or HA-tagged Myd88 and endogenous Ras in HEK293T cells upon **CMA** treatment (6 hours) as measured by ABE, carried out in serum-free media. CNX serves as an assay and loading control ( $n \geq 2$ ). (D) Acyl-biotin exchange (ABE) of HEK293T cells expressing eGFP-tagged GobX and treated with 2BP or **CMA** (0, 20, 50  $\mu$ M) carried out in serum-free or serum-full media. ‘

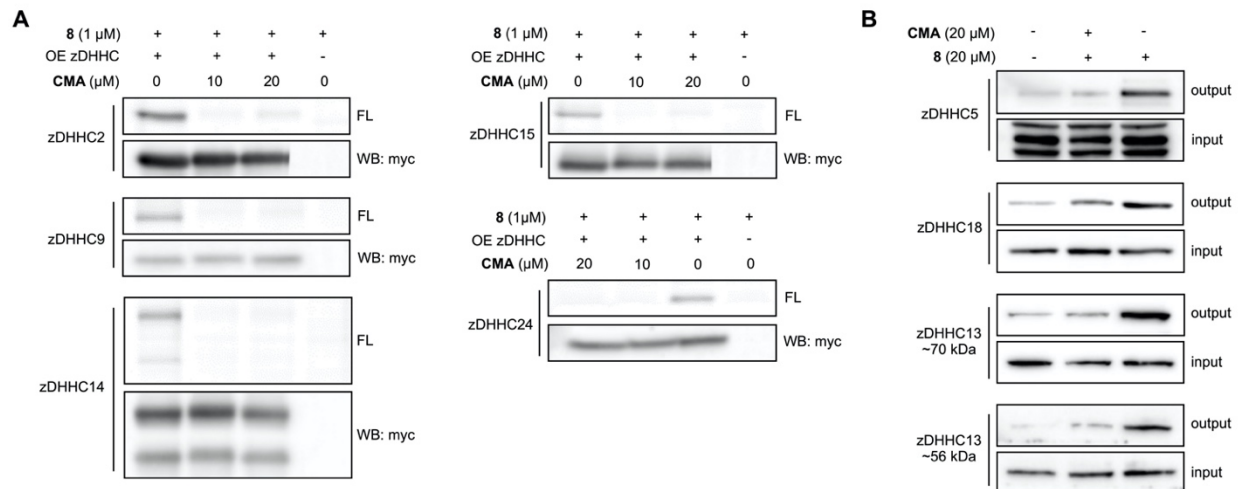


**Figure 4.** Engagement of **CMA** with DHHC family proteins. (A) In-gel fluorescence analysis of myc-tagged DHHC proteins overexpressed in HEK293T cells treated with **CMA** or DMSO (2 hours), followed by labeling with **8** (1  $\mu$ M, 2 hours). Cell lysates subject to click chemistry to conjugate TAMRA-azide to proteins modified by **8**, followed by protein separation via SDS-PAGE. Expression levels visualized via anti-myc tag Western blot ( $n \geq 2$ ). (B) Western blot analysis of endogenous DHHC proteins in HEK293T cells treated with **CMA** or DMSO (3 hours), followed by labeling with **8** (20  $\mu$ M, 3 hours). Cell lysates were subject to click chemistry to conjugate biotin-azide to proteins modified by **8**, followed by streptavidin enrichment, protein separation via SDS-PAGE, and Western blotting for indicated targets ( $n \geq 2$ ).

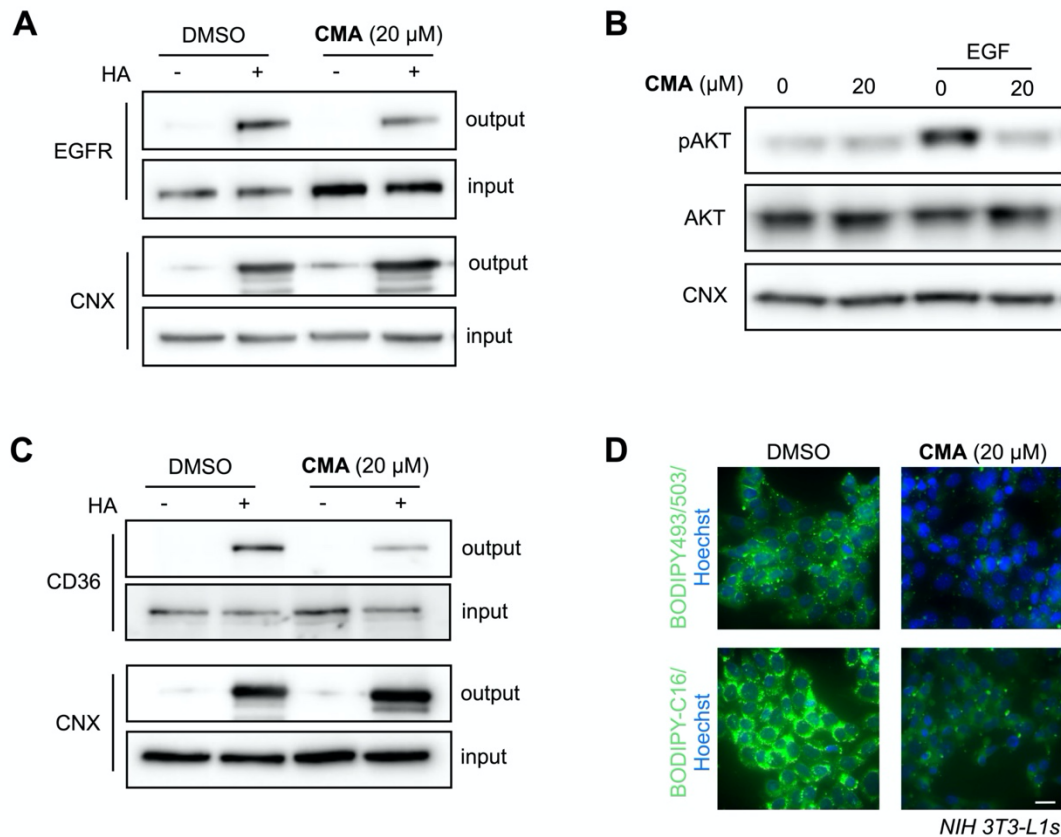


**Figure 5.** Confirmation of **CMA** functional activity *in cellulo*. (A) Analysis of EGFR S-acylation via ABE upon **CMA** treatment (20 μM, 3 hours) in MDA-MB-231 cells, with CNX as an assay and loading control ( $n \geq 2$ ). (B) EGF (100 ng/mL, 15 minutes)-induced phosphorylation of AKT with and without **CMA** treatment (20 μM, 3 hours) ( $n \geq 2$ ). (C) Analysis of CD36 S-acylation via ABE upon **CMA** treatment (20 μM, 6 hours) in 3T3-L1 cells, with CNX as an assay and loading control ( $n \geq 2$ ). (D) Representative images of fluorescence imaging of 3T3-L1 preadipocytes starved (12 hours) and treated with DMSO or **CMA** (20 μM, 3 hours), followed by 10 μM BSA-bound oleate and BODIPY493/503 or BODIPY-palmitate (2 μM, 3 hours) ( $n=5$ ). Scale bar = 20 μM.

## References

1. Blanc, M.; David, F.; Abrami, L.; Migliozi, D.; Armand, F.; Burgi, J.; van der Goot, F. G., SwissPalm: Protein Palmitoylation database. *F1000Res* **2015**, *4*, 261.
2. Lanyon-Hogg, T.; Faronato, M.; Serwa, R. A.; Tate, E. W., Dynamic Protein Acylation: New Substrates, Mechanisms, and Drug Targets. *Trends Biochem Sci* **2017**, *42* (7), 566-581.
3. Linder, M. E.; Deschenes, R. J., Palmitoylation: policing protein stability and traffic. *Nat Rev Mol Cell Biol* **2007**, *8* (1), 74-84.
4. Bhattacharyya, R.; Fenn, R. H.; Barren, C.; Tanzi, R. E.; Kovacs, D. M., Palmitoylated APP Forms Dimers, Cleaved by BACE1. *PLoS One* **2016**, *11* (11), e0166400.
5. Seno, K.; Hayashi, F., Palmitoylation is a prerequisite for dimerization-dependent raftophilicity of rhodopsin. *J Biol Chem* **2017**, *292* (37), 15321-15328.
6. Cao, Y.; Qiu, T.; Kathayat, R. S.; Azizi, S. A.; Thorne, A. K.; Ahn, D.; Fukata, Y.; Fukata, M.; Rice, P. A.; Dickinson, B. C., ABHD10 is an S-depalmitoylase affecting redox homeostasis through peroxiredoxin-5. *Nat Chem Biol* **2019**, *15* (12), 1232-1240.
7. Bolland, D. E.; Moritz, A. E.; Stanislawski, D. J.; Vaughan, R. A.; Foster, J. D., Palmitoylation by Multiple DHHC Enzymes Enhances Dopamine Transporter Function and Stability. *ACS Chem Neurosci* **2019**, *10* (6), 2707-2717.
8. Duncan, J. A.; Gilman, A. G., A cytoplasmic acyl-protein thioesterase that removes palmitate from G protein alpha subunits and p21(RAS). *J Biol Chem* **1998**, *273* (25), 15830-7.
9. Tomatis, V. M.; Trenchi, A.; Gomez, G. A.; Daniotti, J. L., Acyl-protein thioesterase 2 catalyzes the deacylation of peripheral membrane-associated GAP-43. *PLoS One* **2010**, *5* (11), e15045.
10. Lin, D. T.; Conibear, E., ABHD17 proteins are novel protein depalmitoylases that regulate N-Ras palmitate turnover and subcellular localization. *Elife* **2015**, *4*, e11306.
11. Ladygina, N.; Martin, B. R.; Altman, A., Dynamic palmitoylation and the role of DHHC proteins in T cell activation and anergy. *Adv Immunol* **2011**, *109*, 1-44.
12. Jiang, H.; Zhang, X.; Chen, X.; Aramsangtienchai, P.; Tong, Z.; Lin, H., Protein Lipidation: Occurrence, Mechanisms, Biological Functions, and Enabling Technologies. *Chem Rev* **2018**, *118* (3), 919-988.
13. Gok, C.; Fuller, W., Topical review: Shedding light on molecular and cellular consequences of NCX1 palmitoylation. *Cell Signal* **2020**, *76*, 109791.
14. Chen, X.; Ma, H.; Wang, Z.; Zhang, S.; Yang, H.; Fang, Z., EZH2 Palmitoylation Mediated by ZDHHC5 in p53-Mutant Glioma Drives Malignant Development and Progression. *Cancer Res* **2017**, *77* (18), 4998-5010.
15. Beard, R. S., Jr.; Yang, X.; Meegan, J. E.; Overstreet, J. W.; Yang, C. G.; Elliott, J. A.; Reynolds, J. J.; Cha, B. J.; Pivetti, C. D.; Mitchell, D. A.; Wu, M. H.; Deschenes, R. J.; Yuan, S. Y., Palmitoyl acyltransferase DHHC21 mediates endothelial dysfunction in systemic inflammatory response syndrome. *Nat Commun* **2016**, *7*, 12823.
16. Mukai, J.; Liu, H.; Burt, R. A.; Swor, D. E.; Lai, W. S.; Karayiorgou, M.; Gogos, J. A., Evidence that the gene encoding ZDHHC8 contributes to the risk of schizophrenia. *Nat Genet* **2004**, *36* (7), 725-31.
17. Young, E.; Zheng, Z. Y.; Wilkins, A. D.; Jeong, H. T.; Li, M.; Lichtarge, O.; Chang, E. C., Regulation of Ras localization and cell transformation by evolutionarily conserved palmitoyltransferases. *Mol Cell Biol* **2014**, *34* (3), 374-85.
18. Liu, P.; Jiao, B.; Zhang, R.; Zhao, H.; Zhang, C.; Wu, M.; Li, D.; Zhao, X.; Qiu, Q.; Li, J.; Ren, R., Palmitoylacyltransferase Zdhhc9 inactivation mitigates leukemogenic potential of oncogenic Nras. *Leukemia* **2016**, *30* (5), 1225-8.
19. Raymond, F. L.; Tarpey, P. S.; Edkins, S.; Tofts, C.; O'Meara, S.; Teague, J.; Butler, A.; Stevens, C.; Barthorpe, S.; Buck, G.; Cole, J.; Dicks, E.; Gray, K.; Halliday, K.; Hills, K.; Hinton, J.; Jones, D.; Menzies, A.; Perry, J.; Raine, K.; Shepherd, R.; Small, A.; Varian, J.; Widaa, S.; Mallya, U.; Moon, J.; Luo, Y.; Shaw, M.; Boyle, J.; Kerr, B.; Turner, G.; Quarrell, O.; Cole, T.; Easton, D. F.; Wooster, R.; Bobrow, M.; Schwartz, C. E.; Gecz, J.; Stratton, M. R.; Futreal, P. A., Mutations in ZDHHC9, which encodes a palmitoyltransferase of NRAS and HRAS, cause X-linked mental retardation associated with a Marfanoid habitus. *Am J Hum Genet* **2007**, *80* (5), 982-7.

20. Tarpey, P. S.; Smith, R.; Pleasance, E.; Whibley, A.; Edkins, S.; Hardy, C.; O'Meara, S.; Latimer, C.; Dicks, E.; Menzies, A.; Stephens, P.; Blow, M.; Greenman, C.; Xue, Y.; Tyler-Smith, C.; Thompson, D.; Gray, K.; Andrews, J.; Barthorpe, S.; Buck, G.; Cole, J.; Dunmore, R.; Jones, D.; Maddison, M.; Mironenko, T.; Turner, R.; Turrell, K.; Varian, J.; West, S.; Widaa, S.; Wray, P.; Teague, J.; Butler, A.; Jenkinson, A.; Jia, M.; Richardson, D.; Shepherd, R.; Wooster, R.; Tejada, M. I.; Martinez, F.; Carvill, G.; Goliath, R.; de Brouwer, A. P.; van Bokhoven, H.; Van Esch, H.; Chelly, J.; Raynaud, M.; Ropers, H. H.; Abidi, F. E.; Srivastava, A. K.; Cox, J.; Luo, Y.; Mallya, U.; Moon, J.; Parnau, J.; Mohammed, S.; Tolmie, J. L.; Shoubridge, C.; Corbett, M.; Gardner, A.; Haan, E.; Rujirabanjerd, S.; Shaw, M.; Vandeleur, L.; Fullston, T.; Easton, D. F.; Boyle, J.; Partington, M.; Hackett, A.; Field, M.; Skinner, C.; Stevenson, R. E.; Bobrow, M.; Turner, G.; Schwartz, C. E.; Gecz, J.; Raymond, F. L.; Futreal, P. A.; Stratton, M. R., A systematic, large-scale resequencing screen of X-chromosome coding exons in mental retardation. *Nat Genet* **2009**, *41* (5), 535-43.
21. Runkle, K. B.; Kharbanda, A.; Stypulkowski, E.; Cao, X. J.; Wang, W.; Garcia, B. A.; Witze, E. S., Inhibition of DHHC20-Mediated EGFR Palmitoylation Creates a Dependence on EGFR Signaling. *Mol Cell* **2016**, *62* (3), 385-396.
22. Kharbanda, A.; Walter, D. M.; Gudiel, A. A.; Schek, N.; Feldser, D. M.; Witze, E. S., Blocking EGFR palmitoylation suppresses PI3K signaling and mutant KRAS lung tumorigenesis. *Sci Signal* **2020**, *13* (621).
23. Sanders, S. S.; Hayden, M. R., Aberrant palmitoylation in Huntington disease. *Biochem Soc Trans* **2015**, *43* (2), 205-10.
24. Roth, A. F.; Feng, Y.; Chen, L.; Davis, N. G., The yeast DHHC cysteine-rich domain protein Akr1p is a palmitoyl transferase. *J Cell Biol* **2002**, *159* (1), 23-8.
25. Lobo, S.; Greentree, W. K.; Linder, M. E.; Deschenes, R. J., Identification of a Ras palmitoyltransferase in *Saccharomyces cerevisiae*. *J Biol Chem* **2002**, *277* (43), 41268-73.
26. Fukata, M.; Fukata, Y.; Adesnik, H.; Nicoll, R. A.; Brecht, D. S., Identification of PSD-95 palmitoylating enzymes. *Neuron* **2004**, *44* (6), 987-96.
27. Wang, J.; Hao, J. W.; Wang, X.; Guo, H.; Sun, H. H.; Lai, X. Y.; Liu, L. Y.; Zhu, M.; Wang, H. Y.; Li, Y. F.; Yu, L. Y.; Xie, C.; Wang, H. R.; Mo, W.; Zhou, H. M.; Chen, S.; Liang, G.; Zhao, T. J., DHHC4 and DHHC5 Facilitate Fatty Acid Uptake by Palmitoylating and Targeting CD36 to the Plasma Membrane. *Cell Rep* **2019**, *26* (1), 209-221 e5.
28. Abrami, L.; Dallavilla, T.; Sandoz, P. A.; Demir, M.; Kunz, B.; Savoglidis, G.; Hatzimanikatis, V.; van der Goot, F. G., Identification and dynamics of the human ZDHHC16-ZDHHC6 palmitoylation cascade. *Elife* **2017**, *6*.
29. Davda, D.; El Azzouny, M. A.; Tom, C. T.; Hernandez, J. L.; Majmudar, J. D.; Kennedy, R. T.; Martin, B. R., Profiling targets of the irreversible palmitoylation inhibitor 2-bromopalmitate. *ACS Chem Biol* **2013**, *8* (9), 1912-7.
30. Pedro, M. P.; Vilcaes, A. A.; Tomatis, V. M.; Oliveira, R. G.; Gomez, G. A.; Daniotti, J. L., 2-Bromopalmitate reduces protein deacylation by inhibition of acyl-protein thioesterase enzymatic activities. *PLoS One* **2013**, *8* (10), e75232.
31. Tian, L.; McClafferty, H.; Jeffries, O.; Shipston, M. J., Multiple palmitoyltransferases are required for palmitoylation-dependent regulation of large conductance calcium- and voltage-activated potassium channels. *J Biol Chem* **2010**, *285* (31), 23954-62.
32. Zheng, B.; Zhu, S.; Wu, X., Clickable analogue of cerulenin as chemical probe to explore protein palmitoylation. *ACS Chem Biol* **2015**, *10* (1), 115-21.
33. DeJesus, G.; Bizzozero, O. A., Effect of 2-fluoropalmitate, cerulenin and tunicamycin on the palmitoylation and intracellular translocation of myelin proteolipid protein. *Neurochem Res* **2002**, *27* (12), 1669-75.
34. Jennings, B. C.; Nadolski, M. J.; Ling, Y.; Baker, M. B.; Harrison, M. L.; Deschenes, R. J.; Linder, M. E., 2-Bromopalmitate and 2-(2-hydroxy-5-nitro-benzylidene)-benzo[b]thiophen-3-one inhibit DHHC-mediated palmitoylation in vitro. *J Lipid Res* **2009**, *50* (2), 233-42.
35. Jackson, P. A.; Widen, J. C.; Harki, D. A.; Brummond, K. M., Covalent Modifiers: A Chemical Perspective on the Reactivity of alpha,beta-Unsaturated Carbonyls with Thiols via Hetero-Michael Addition Reactions. *J Med Chem* **2017**, *60* (3), 839-885.

36. Lanyon-Hogg, T.; Ritzefeld, M.; Sefer, L.; Bickel, J. K.; Rudolf, A. F.; Panyain, N.; Bineva-Todd, G.; Ocasio, C. A.; O'Reilly, N.; Siebold, C.; Magee, A. I.; Tate, E. W., Acylation-coupled lipophilic induction of polarisation (Acyl-cLIP): a universal assay for lipid transferase and hydrolase enzymes. *Chem Sci* **2019**, *10* (39), 8995-9000.
37. Qiu, T.; Kathayat, R. S.; Cao, Y.; Beck, M. W.; Dickinson, B. C., A Fluorescent Probe with Improved Water Solubility Permits the Analysis of Protein S-Depalmitoylation Activity in Live Cells. *Biochemistry* **2018**, *57* (2), 221-225.
38. Martin, B. R.; Cravatt, B. F., Large-scale profiling of protein palmitoylation in mammalian cells. *Nat Methods* **2009**, *6* (2), 135-8.
39. Drisdell, R. C.; Green, W. N., Labeling and quantifying sites of protein palmitoylation. *Biotechniques* **2004**, *36* (2), 276-85.
40. Kim, Y. C.; Lee, S. E.; Kim, S. K.; Jang, H. D.; Hwang, I.; Jin, S.; Hong, E. B.; Jang, K. S.; Kim, H. S., Toll-like receptor mediated inflammation requires FASN-dependent MYD88 palmitoylation. *Nat Chem Biol* **2019**, *15* (9), 907-916.
41. Lin, Y. H.; Doms, A. G.; Cheng, E.; Kim, B.; Evans, T. R.; Machner, M. P., Host Cell-catalyzed S-Palmitoylation Mediates Golgi Targeting of the Legionella Ubiquitin Ligase GdbX. *J Biol Chem* **2015**, *290* (42), 25766-81.
42. Dallavilla, T.; Abrami, L.; Sandoz, P. A.; Savoglidis, G.; Hatzimanikatis, V.; van der Goot, F. G., Model-Driven Understanding of Palmitoylation Dynamics: Regulated Acylation of the Endoplasmic Reticulum Chaperone Calnexin. *PLoS Comput Biol* **2016**, *12* (2), e1004774.
43. Martin, B. R., Chemical approaches for profiling dynamic palmitoylation. *Biochem Soc Trans* **2013**, *41* (1), 43-9.
44. Jennings, B. C.; Linder, M. E., DHHC protein S-acyltransferases use similar ping-pong kinetic mechanisms but display different acyl-CoA specificities. *J Biol Chem* **2012**, *287* (10), 7236-45.
45. Mitchell, D. A.; Mitchell, G.; Ling, Y.; Budde, C.; Deschenes, R. J., Mutational analysis of *Saccharomyces cerevisiae* Erf2 reveals a two-step reaction mechanism for protein palmitoylation by DHHC enzymes. *J Biol Chem* **2010**, *285* (49), 38104-14.
46. Zheng, B.; DeRan, M.; Li, X.; Liao, X.; Fukata, M.; Wu, X., 2-Bromopalmitate analogues as activity-based probes to explore palmitoyl acyltransferases. *J Am Chem Soc* **2013**, *135* (19), 7082-5.
47. Bastin, G.; Dissanayake, K.; Langburt, D.; Tam, A. L. C.; Lee, S. H.; Lachhar, K.; Heximer, S. P., RGS4 controls Gα<sub>q</sub>-mediated regulation of Bcl-2 phosphorylation on TGN38-containing intracellular membranes. *J Cell Sci* **2020**, *133* (12).
48. Zhang, Y.; Lin, Z.; Tan, Y.; Bu, F.; Hao, P.; Zhang, K.; Yang, H.; Liu, S.; Ren, Y., Exploration of Missing Proteins by a Combination Approach to Enrich the Low-Abundance Hydrophobic Proteins from Four Cancer Cell Lines. *J Proteome Res* **2020**, *19* (1), 401-408.
49. Hao, J. W.; Wang, J.; Guo, H.; Zhao, Y. Y.; Sun, H. H.; Li, Y. F.; Lai, X. Y.; Zhao, N.; Wang, X.; Xie, C.; Hong, L.; Huang, X.; Wang, H. R.; Li, C. B.; Liang, B.; Chen, S.; Zhao, T. J., CD36 facilitates fatty acid uptake by dynamic palmitoylation-regulated endocytosis. *Nat Commun* **2020**, *11* (1), 4765.
50. Arnott, J. A.; Planey, S. L., The influence of lipophilicity in drug discovery and design. *Expert Opin Drug Discov* **2012**, *7* (10), 863-75.
51. Yao, H.; Lan, J.; Li, C.; Shi, H.; Brosseau, J. P.; Wang, H.; Lu, H.; Fang, C.; Zhang, Y.; Liang, L.; Zhou, X.; Wang, C.; Xue, Y.; Cui, Y.; Xu, J., Inhibiting PD-L1 palmitoylation enhances T-cell immune responses against tumours. *Nat Biomed Eng* **2019**, *3* (4), 306-317.
52. Yao, H.; Li, C.; He, F.; Song, T.; Brosseau, J.-P.; Wang, H.; Lu, H.; Fang, C.; Shi, H.; Lan, J.; Fang, J.-Y.; Xu, J., A peptidic inhibitor for PD-1 palmitoylation targets its expression and functions. *RSC Chemical Biology* **2021**.